HHS Public Access

Author manuscript

Adv Ther (Weinh). Author manuscript; available in PMC 2023 October 01.

Published in final edited form as:

Adv Ther (Weinh). 2022 October ; 5(10): . doi:10.1002/adtp.202200092.

A single-dose Qβ VLP vaccine against S100A9 protein reduces atherosclerosis in a preclinical model

Oscar A. Ortega-Rivera[1,2], **Matthew D. Shin**[1,2], **Miguel A. Moreno-Gonzalez**[1,2], **Jonathan K. Pokorski**[1,2,3], **Nicole F. Steinmetz**[1,2,3,4,5,6,*]

[1]Department of NanoEngineering, University of California-San Diego, La Jolla CA 92039, USA

[2]Center for Nano-ImmunoEngineering, University of California-San Diego, La Jolla CA 92039, USA

[3]Institute for Materials Discovery and Design, University of California-San Diego, La Jolla CA 92039, USA

[4]Department of Bioengineering, University of California-San Diego, La Jolla CA 92039, USA

[5]Department of Radiology, University of California-San Diego, La Jolla CA 92039, USA

[6]Moores Cancer Center, University of California-San Diego, La Jolla CA 92039, USA

Abstract

The standard therapy for cardiovascular disease (CVD) is the administration of statins to reduce plasma cholesterol levels, but this requires lifelong treatment. We developed a CVD vaccine candidate that targets the pro-inflammatory mediator calprotectin by eliciting antibodies against the S100A9 protein. The vaccine, based on bacteriophage Qβ virus-like particles (VLPs) displaying S100A9 peptide epitopes, was formulated as a slow-release PLGA:VLP implant by hot-melt extrusion. The single-dose implant elicited S100A9-specific antibody titers comparable to a three-dose injection schedule with soluble VLPs. In an animal model of CVD ($ApoE^{-/-}$ mice fed on a high-fat diet), the implant reduced serum levels of calprotectin, IL-1β, IL-6 and MCP-1, resulting in less severe aortic lesions. This novel implant was therefore able to attenuate atherosclerosis over a sustained period and offers a novel and promising strategy to replace the repetitive administration of statins for the treatment of CVD.

Graphical Abstract

* nsteinmetz@ucsd.edu .

Author Contributions

All authors contributed to the writing of this manuscript and have approved the final version of the manuscript.

Conflict of Interest

Drs. Steinmetz and Pokorski are co-founders of, have equity in, and have a financial interest with Mosaic ImmunoEngineering Inc. Dr. Pokorski serves as scientific advisor and paid consultant to Mosaic; Dr. Steinmetz serves as Director, Board Member, and Acting Chief Scientific Officer, and paid consultant to Mosaic. The other authors declare no potential conflicts of interest.

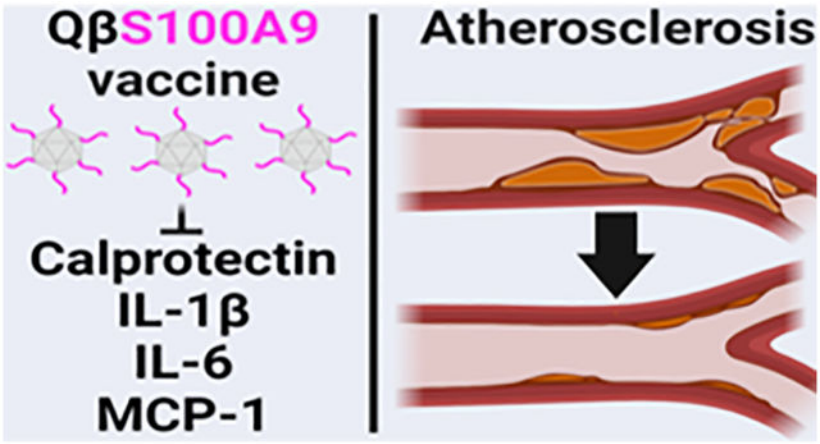

We developed a cardiovascular disease vaccine candidate that targets the pro-inflammatory mediator calprotectin by eliciting antibodies against the S100A9 protein. The vaccine, virus-like particles displaying S100A9 peptide epitopes, was formulated as a slow-release PLGA:VLP implant. Using a preclinical model, we demonstrate that vaccination results in long-lasting and specific anti-S100A9 antibodies – lowering S100A9 levels as well as pro-atherogenic cytokines levels, and therefore limiting atherosclerosis development.

Keywords

S100A9; calprotectin; vaccine; virus-like particle; atherosclerosis

INTRODUCTION

Cardiovascular disease (CVD) is the leading cause of mortality worldwide, with ~18 million CVD-related fatalities in 2019 representing 31% of all deaths[1]. The major underlying cause of cardiovascular events is atherosclerosis, a chronic inflammatory disease that develops in response to lipid accumulation, with an autoimmune component[2,3]. The gold standard treatment for atherosclerosis is the administration of statins to reduce plasma levels of low-density lipoprotein-cholesterol (LDL-C)[3]. However, many atherosclerosis patients remain at risk due to chronic inflammation[4,5]. This reflects the activity of pro-atherogenic cytokines such as interleukin (IL)-1β and IL-6, and chemokines such as monocyte chemoattractant protein-1 (MCP-1), which are secreted by macrophages, lymphocytes, natural killer cells, and vascular smooth muscle cells during the development of atherosclerosis[6,7]. Several pro-inflammatory and pro-atherogenic cytokines have been targeted in CVD clinical trials, highlighting the relevance of anti-inflammatory therapy for the management of atherosclerosis[6].

Another promising therapeutic target is the inflammatory biomarker calprotectin, which promotes cytokine secretion in multiple inflammatory diseases[8]. Calprotectin is a heterodimer of the calcium-modulated proteins S100A8 and S100A9, also known as myeloid-related protein (MRP)-8 and MRP-14, and is secreted mainly by neutrophils[9]. S100 family proteins regulate myeloid cell function, and control inflammation in part by

activating Toll-like receptor-4 (TLR-4)[10], the receptor for advanced glycation end products (RAGE)[11] and the extracellular matrix metalloprotease inducer (EMMPRIN)[12]. Elevated levels of calprotectin are found systemically in patients with acute coronary syndromes (ACS), and also at the sites of coronary occlusion and in atherosclerotic plaques[13,14,15,16]. In longitudinal studies, calprotectin is a positive marker of CVD and is independent of established risk factors[17].

Transcriptional profiling has shown that S100A9, one of the components of the calprotectin heterodimer, is an important regulator of vascular inflammation and atherothrombosis[14]. The corresponding gene was therefore knocked out in the ApoE$^{-/-}$ mouse model of atherosclerosis, resulting in attenuated atherosclerotic lesion formation and plaque inflammation when the ApoE$^{-/-}$ S100A9$^{-/-}$ double knockouts were fed on a high-fat diet, predominantly due to the regulation of vascular inflammation and vascular injury promoted by leukocyte recruitment[18]. Calprotectin-associated damage during atherosclerosis can therefore be ameliorated by targeting S100A9. Furthermore, the S100A9-null mice developed normal organs and tissues, and had a normal lifespan[19], suggesting that S100A9 is a suitable target for CVD interventional therapy.

Passive immunization (monoclonal antibody therapy) against pro-atherogenic cytokines such as IL-1β[20] and TNF-α[21] was shown to reduce the risk of cardiovascular events. Furthermore, the US Food and Drug Administration recently approved the monoclonal antibodies alirocumab and evolocumab targeting the proprotein convertase subtilisin/kexin-9 (PCSK9), a cholesterol metabolism checkpoint protein[22,23,24]. However, passive immunotherapy requires repeated dosing and lifelong treatment, which is too expensive for many patients[25]. Active immunotherapy (vaccination) is a cost-effective approach that should achieve similar protective effects. Atherosclerosis vaccines should therefore focus on one of two major objectives: (1) lowering serum LDL-C levels, or (2) attenuating the chronic inflammatory response[26].

To address the second objective, we developed a CVD vaccine targeting the S100A9 protein to reduce serum levels of calprotectin. The success of any vaccine requires the use of a suitable antigen combined with a strong adjuvant and an effective delivery strategy. We therefore used virus-like particles (VLPs) from bacteriophage Qβ to display a B-cell epitope from the mouse S100A9 protein (Figure 1). VLP vaccines have shown efficacy against other self-antigen epitopes (ApoB, CETP and PCSK9)[27] as well as pathogen epitopes from human papillomavirus (HPV)[28] and SARS-CoV-2[29]. Qβ VLPs are macromolecular display platforms for foreign epitopes attached by conjugation or genetic fusion, and they act as a built-in adjuvant to enhance the stability of antigens and enable lymphatic trafficking and processing by antigen presenting cells[30,31]. Qβ VLPs can be produced in large quantities by the expression of a recombinant Qβ 14-kDa capsid protein in *Escherichia coli* (in vivo assembly), and scalable production according to current good manufacturing practices (cGMP) has been demonstrated for several Qβ-based VLP vaccine candidates in clinical trials[31]. To prolong the delivery of the vaccine, we opted for a slow-release poly(lactic-*co*-glycolic acid) (PLGA) implant, which was mixed with the VLP vaccines using hot melt-extrusion. This process does not compromise the structural properties or immunogenicity of the vaccine[28,29,32,33,34]. We tested the efficacy and safety of the vaccine in a traditional

prime-boost-boost schedule vs the single-dose slow-release injectable implant in healthy mice and in the ApoE$^{-/-}$ model of atherosclerosis by measuring antibody titers and immune responses, plasma levels of calprotectin, IL-1β, IL-6, and MCP-1, and the severity of aortic lesions in the aortic arch and thoracic aorta.

RESULTS AND DISCUSSION

Characterization of QβS100A9 particles

We chose S100A9 epitope $_{101}$RGHGHSHGKG$_{110}$ (Figure 1) based on its score (0.5 threshold) as a B-cell epitope as determined using the BepiPred-2.0 Sequential B-Cell Epitope Predictor[35]. In a previous study using a similar approach to treat thrombosis[36], the authors used epitope $_{104}$GHSHGKGCGK$_{113}$, which includes amino acids 111–113 (CGK), but we found that those residues did not pass the score threshold and we excluded them. The epitope $_{101}$RGHGHSHGKG$_{110}$ was fused to the C-terminus of the Qβ coat protein (CP) with an intervening GSG linker, and was expressed in a vector also containing the unmodified Qβ CP gene to allow the assembly of hybrid particles (Figure 2A) as previously described[27,35]. The QβS100A9 vaccine candidate was expressed in *E. coli* and purified by sucrose gradient ultracentrifugation, with yields of ~360 mg unmodified Qβ and ~195 mg QβS100A9 per liter of culture. The lower yield of hybrid particles has been observed before, and probably reflects the negative impact of the additional peptide on VLP assembly[27].

Sodium dodecyl sulfate-polyacrylamide gel electrophoresis (SDS-PAGE) analysis (Figure 2B) confirmed that only wild-type CP (~14 kDa) was present in the unmodified Qβ VLPs, whereas the hybrid particles contained both the wild-type CP and the larger QβS100A9 CP (~15.2 kDa). Densitometric comparison revealed that the hybrid particles were composed of 42–50% QβS100A9 CPs, indicating that 77–90 peptide epitopes are displayed per hybrid VLP (180 CP subunits in total) (Figure 2C). Dynamic light scattering (DLS) revealed the particles were monodisperse with a hydrodynamic diameter (Z-average) of ~32 nm for unmodified Qβ VLPs and ~39 nm for QβS100A9 VLPs (Figure 2D). Fast protein liquid chromatography (FPLC) revealed slightly overlapping major single peaks for unmodified Qβ and QβS100A9, with a similar elution volume of 10–15 mL indicating that both types of VLP were intact and did not form significant or apparent aggregates (Figure 2E). The unmodified Qβ VLPs had a higher polydispersity index (PDI) of 0.11 compared to 0.01 for the QβS100A9 VLPs, indicating that the QβS100A9 particles were larger but more uniformly distributed, as reported for other Qβ-based vaccines[27]. Transmission electron microscopy (TEM) of negatively-stained particles indicated that the Qβ and QβS100A9 VLPs were intact (Figure 2F). These results confirm that the QβS100A9 VLPs are stable and the peptide does not affect particle integrity.

Immunogenicity of soluble QβS100A9 VLPs and slow-release implants

We previously reported slow-release formulations for vaccines against HPV, COVID-19 and cholesterol-related proteins associated with CVD, and we developed protocols for hot-melt extrusion yielding degradable PLGA:Qβ implants with a ~1 month release timeframe that achieved the same immunogenicity as a multi-dose regimen of soluble vaccines[27,28,29]. To confirm the immunogenicity of the VLPs before formulation, we compared the soluble

QβS100A9 VLPs to the free peptide epitope in a traditional subcutaneous (s.c.) vaccination schedule consisting of a prime plus two boosts, 2 weeks apart. Each injection consisted of 100 μg QβS100A9 VLPs or 5 μg of the free peptide, resulting in a molar equivalent dosage of the epitope in each case (Figure 3A). As expected, the QβS100A9 VLPs elicited significantly higher specific IgG titers than the free peptide over a period of 12 weeks (Figure 3B), confirming the adjuvant activity of the VLPs[40].

Next, we produced slow-release implants (80% PLGA, 10% VLPs and 10% PEG8000) containing either unmodified Qβ (control) or QβS100A9 VLPs. Hot-melt extrusion yielded injectable implant rods. The implants contained 300 μg of VLPs to match the combined dose of the prime plus two boosts schedule (Figure 3E). As expected, the IgG titers against the S100A9 epitope were significantly higher in the PLGA/QβS100A9 VLP group than the control VLP group over a period of 20 weeks (Figure 3F). The IgG titers in the PLGA/QβS100A9 implant VLP group were similar to those in the soluble QβS100A9 VLP group (~10^4), confirming that a single dose of the PLGA/QβS100A9 implant is effective (Figure 3B,F). From a clinical perspective, the single-dose implant favors patient compliance and reduces the healthcare burden by offering the potential for long-acting vaccines whose release rate can be tailored based on the polymer composition[41].

We next evaluated the immunoglobulin subtypes elicited by the vaccine formulations. IgG2b is a subclass of IgG induced primarily by Th1-type cytokines such as interferon gamma (IFN-γ), whereas IgG1 antibodies are induced by Th2-type cytokines such as IL-4[40,42]. The soluble VLPs resulted in an IgG1/IgG2b ratio < 1 that persisted over 12 weeks, indicating a Th1-biased profile (Figure 3D). In contrast, the implant resulted in a marked Th1 bias initially, but this trended toward a balanced Th1/Th2 response by week 15 (Figure 3H). We also observed that IgM titers declined over time following vaccination with soluble VLPs but increased over time following vaccination with the implant, indicating that the slow release maintains a constant boosting effect that influences the levels of IgM and other immunoglobulins (Figure 3C,G). We have previously observed sustained high levels of IgM with other vaccines formulated as implants[29].

Given that S100A9 belongs to a large family of S100 proteins with similar structures and shared domains[36], we selected an epitope unique to S100A9 to avoid off-target effects. To confirm the specificity of the antibodies elicited by the QβS100A9 vaccine, we tested their ability to bind S100A8, S100A9 and S100A8/9 heterodimers in dot blot assays. As expected, plasma from QβS100A9-vaccinated mice only recognized S100A9 and the heterodimer S100A8/9, but not the S100A8 protein (Figure 4). Antibodies from mice injected with the free peptide generated weaker signals but we observed the same overall result (Figure 4).

Safety of soluble QβS100A9 VLPs and slow-release implants

S100A9 is a self-antigen, so immunotoxicity parameters such as the absence of a target-specific T-cell response (Th and cytotoxic T cells) are desirable[43,44,45]. We therefore used ELISpot assays to evaluate the activation of primed T cells following vaccination with soluble QβS100A9 VLPs or the implant. We monitored the production of IFN-γ (linked to Th1-biased profiles) and IL-4 (linked to Th2-biased profiles) in splenocytes isolated 4

weeks after the second 100-μg dose of soluble QβS100A9 or a single 200-μg dose of the QβS100A9 implant, and also in splenocytes from naïve mice.

IFN-γ was significantly more abundant in the splenocytes of vaccinated (soluble or implant) and naïve mice following stimulation with recombinant mouse S100A9, but not following stimulation with the free peptide (Figure 5A–C). The detection of this response even in naïve splenocytes indicates that the S100A9 monomer and S100A8/9 heterodimer act as damage associated molecular patterns (DAMPs) via their ability to bind the RAGE, TLR-4 and EMMPRIN receptors, leading to MAPK signaling and the translocation of NF-κβ from the cytosol to the nucleus, triggering the activation of genes that control inflammation[46,47]. This result makes it difficult to determine whether the presence of T cells primed with the S100A9 epitope could exacerbate the T cell response because even naïve splenocytes are activated in the presence of S100A9. However, the IFN-γ SFCs were more abundant on splenocytes from mice vaccinated with the soluble VLPs, which agrees with the persistent Th1-biased profile revealed by the IgG1/IgG2b ratio (Figure 3C,D). On the other hand, the IFN-γ SFCs observed on splenocytes from mice vaccinated with the implant (Figure 5B) showed a response comparable to that of naïve splenocytes, reflecting the balanced Th1/Th2 profile (Figure 3G,H).

The stimulation of splenocytes with unmodified Qβ VLPs resulted in a significant increase in IFN-γ compared to the non-stimulated control (medium only), indicating a strong response to the VLP scaffold[27,29]. The phorbol 12-myristate 13-acetate (PMA)/ionomycin positive control was the only stimulant that triggered the significant production of both IFN-γ and IL-4 by splenocytes from all vaccinated and naïve mice. Accordingly, we decided to study the PLGA-based QβS100A9 implant in more detail, given its more balanced Th1/Th2 response and its IgG titers comparable to the soluble VLPs. Most Qβ VLP vaccines developed by us[27] and others[44] triggered a Th2-biased response, but this is likely to be epitope-dependent given the Th1-biased response reported for a Qβ VLP self-antigen vaccine against epitopes derived from different loops of the C3 domain of IgE that binds to the high-affinity FcεRI receptor[48]. The Th1-biased response was dependent on TLR-7 activation because TLR-7 knockout mice switched to a Th2-biased profile[48]. We found that the Th response can be modulated by delivering the vaccine as a slow-release implant, probably reflecting the constant release of small quantities of VLPs during implant biodegradation.

We also assessed the safety of the vaccines by measuring the concentration of kidney injury molecule 1 (KIM-1), a transmembrane glycoprotein and biomarker of kidney injury[49], as well as the plasma activity of aspartate aminotransferase (AST) and alanine transaminase (ALT), which are biomarkers of liver injury[50]. We compared mice vaccinated with QβS100A9 VLPs vs controls after 12 weeks, but observed no significant changes on the normal range[51] of KIM-1 or AST/ALT activity (Figure 5D). We can therefore confirm that the QβS100A9 VLPs neither altered kidney physiology nor caused liver injury.

Efficacy of QβS100A9 slow-release implants against atherosclerosis

Having confirmed the immunogenicity and safety of the QβS100A9 VLPs and implants in healthy animals, we tested the efficacy of the QβS100A9 implant in ApoE$^{-/-}$ mice fed

on a high-fat western diet as a model of atherosclerosis. We selected the implant because it can be administered as a single dose but it elicits antibody titers similar to the soluble VLPs while generating a more balanced Th1/Th2 profile. Mice were immunized once with the QβS100A9 implant or the unmodified Qβ implant as a control and were monitored for 24 weeks, the first 4 weeks on a regular diet before switching at the beginning of week 5 to the high-fat diet (Figure 6A). S100A9-specific IgG appeared during week 2, and titers remained stable until week 8 and then increased slightly between weeks 8 and 12 (Figure 6B). As expected, the QβS100A9 group elicited significantly higher titers than the control group at all time points. We assessed the IgG1/IgG2b ratio and observed a similar profile to that observed for healthy mice. In more detail, we observed a Th1-biased profile (IgG1/IgG2b < 1) for all except one of the mice at week 4. Most profiles remained the same at week 8, except one mouse with a balanced Th1/Th2 profile and two trending toward a Th2-biased response. Finally, three of the mice showed a Th2-biased response by week 24, two showed a balanced Th1/Th2 response, and five retained their Th1-biased profile (Figure 6C). Additionally, as observed in the healthy animals, IgM levels remained high throughout the experiment (Figure 6D). These data confirmed that the QβS100A9 implant behaves similarly in healthy and atherosclerotic mice.

The QβS100A9 implant ameliorates aortic lesions by reducing the plasma levels of calprotectin and pro-inflammatory cytokines

We measured the degree of plaque formation on the aortas of mice fed on the high-fat western diet by standard oil red O staining, which detects neutral fat, fatty acids and triglycerides[52] that accumulate in atherosclerotic plaques but not in the healthy endothelium. The positive staining is directly correlated to atherosclerosis and can be quantified as the percentage of lesion in the aortas (Figure 7C and Supp. Figure 1). We found that the percentage of lesion in the QβS100A9 vaccine implant group (21.5 ± 2%) was 32% lower than that in the control group (31.6 ± 3%). This is noteworthy because double knockout animals ($ApoE^{-/-}$ $S100A9^{-/-}$) fed on a high-fat diet showed a 25–30% reduction in lesion area in the thoracic and abdominal aorta[18], suggesting that blocking S100A9 activity either by gene knockout or vaccination may reduce the level of S100A9 in the plasma, thus preventing calprotectin from signaling via TLR-4[53] and modulating calcium signaling[19], reorganizing the cytoskeleton[54] and triggering the release of pro-inflammatory cytokines.

To determine the mechanism of action, we measured the levels of calprotectin in the plasma. We found significantly lower levels in the QβS100A9 group compared to controls at all time points, reaching a maximum differential of 3.3-fold during week 12 (Figure 7D). In addition to atherosclerosis and CVD[13,14,17,55], calprotectin is an important biomarker for the diagnosis and monitoring of many other inflammatory diseases[8] because it stimulates the production of pro-inflammatory cytokines/chemokines such as IL-1β[56], IL-6 and MCP-1[57]. IL-1β is key mediator of the pro-inflammatory response. Higher levels of this cytokine are found in atherosclerotic human arteries compared to healthy controls and its abundance positively correlates with disease severity[58]. IL-1β activates secondary inflammatory mediators such as IL-6 and triggers pro-coagulant activity, the expression of adhesion molecules required for leukocyte recruitment, and the production of MCP-1[59,60]. Together these changes promote the recruitment of monocytic phagocytes, which are strongly

implicated in atherogenesis[61]. IL-1β deficiency attenuated the spontaneous development of atherosclerotic lesions in ApoE$^{-/-}$ mice[62]. We found that the lower levels of calprotectin in the QβS100A9 group correlated with lower levels of IL-1β, IL-6 and MCP-1 (Figure 7E–G). These cytokines/chemokines were also depleted in ApoE$^{-/-}$ S100A9$^{-/-}$ double knockout mice, correlating with the less severe aortic lesions[18].

The precise mechanism by which the S100A9-specific antibodies reduce the severity of lesions is unclear. When a similar epitope was used to treat thrombosis in mice ($_{104}$GHSHGKGCGK$_{113}$, from mouse S100A9) and monkeys ($_{102}$GHHHKPGLGE$_{111}$, from monkey S100A9), the promising results were attributed to the inhibition of S100A9/CD36 signaling in platelets[36,63]. Many pro-inflammatory cytokines are triggered by S100A9/TLR-4 signaling, but a recent study showed that 73–85 amino acids in S100A9 specifically interact with TLR-4 and trigger TNF-α expression[53]. Our data show that the depletion of calprotectin is sufficient to reduce the secretion of pro-inflammatory cytokines/chemokines and is therefore protective against aortic lesions, without knowing which S100A9-dependent signaling pathway is blocked by the antibodies.

Interestingly, the QβS100A9 implant did not affect plasma levels of calprotectin in healthy animals on a regular diet (Supp. Figure 2) but prevented the levels from increasing when these animals were fed on the high-fat diet (Figure 7D). This is important because calprotectin also protects against pathogens[64], and it would be undesirable to completely remove a beneficial defense mechanism. Accordingly, we measured other health-related parameters beyond the severity of aortic lesions and cytokine levels. We observed no significant differences in body weight between the treatment groups at any point during the experiment, which was anticipated because the vaccine does not affect food intake (Figure 7A). However, around the middle of the study (week 12) we observed a significantly higher amount of total cholesterol in the QβS100A9 vaccine group (1130 ± 44 mg/dL) compared to the control (996 ± 31 mg/dL), but this relationship switched by week 24, with the QβS100A9 vaccine group (878 ± 60 mg/dL) showing a significantly lower amount of total cholesterol than the controls (1158 ± 94 mg/dL) (Figure 7B). The relationship between systemic S100A9 and cholesterol homeostasis is unclear, and would be an important subject for further investigation. We found no significant difference in the weights of individual organs between the QβS100A9 vaccine group and controls (Supp. Figure 3).

Conclusion

In summary, our single-dose QβS100A9 vaccine formulated as a PLGA:VLP implant successfully reduced the extent of aortic lesions in a model of atherosclerosis, most likely by depleting calprotectin and thus preventing the secretion of pro-inflammatory cytokines/chemokines such as IL-1β, IL-6 and MCP-1. This was achieved without apparent systemic damage or adverse autoimmune responses. Calprotectin remained at normal basal levels in healthy mice. The effect of the vaccine was to deplete calprotectin only in the disease state, when unvaccinated animals experienced elevated levels. This promising anti-atherosclerosis vaccine offers a novel approach for the management of CVD and other inflammatory diseases and should now be tested in larger mammals and human clinical trials.

METHODS

Production of Qβ VLPs.

Bacteriophage Qβ VLPs were expressed as previously reported[27,29,65]. Genes encoding the wild-type Qβ CP (NCBI accession: P03615) and CP fused to the mouse S100A9 epitope $_{101}$RGHGHSHGKG$_{110}$ (NCBI accession: P31725) were codon optimized for *E. coli* and inserted into the expression vector pCOLA-DUET1 by GenScript Biotech. A linker (GSG) was placed between the C-terminus of the CP and the N-terminus of the peptide. The final vector was named pCOLA_Qβ_QβS100A9. As a control for some experiments, we used vector pCDF_Qβ carrying only the wild-type Qβ CP gene[27]. *E. coli* Bl21 (DE3) cells (New England BioLabs) transformed with pCDF_Qβ or pCOLA_Qβ_QβS100A9 were grown at 37 °C for 16 h shaking at 250 rpm in 10 mL MagicMedia (Invitrogen) with the appropriate antibiotics: 25 μg/mL streptomycin (Sigma-Aldrich) for pCDF_Qβ and 50 μg/mL kanamycin (Sigma-Aldrich) for pCOLA_Qβ_QβS100A9. The culture was scaled up to 200 mL in the same medium and incubated at 37 °C for 20 h, shaking at 300 rpm. The cells were pelleted by centrifugation (5000 × *g*, 20 min, 4 °C) and frozen at −80 °C overnight. The pellet was then lysed by resuspending it in 10 mL lysis buffer (GoldBio) per gram of wet mass, adding a lysis cocktail comprising 1 mg/mL lysozyme (GoldBio), 2 μg/mL DNase (Promega) and 2 mM $MgCl_2$, and incubating at 37 °C for 1 h before sonicating at 30% amplitude for 10 min on ice, with 5-s pulses interspersed with 5-s gaps. The lysate was centrifuged (5000 × *g*, 30 min, 4 °C) and the clear supernatant was set aside. Unmodified Qβ VLPs and hybrid QβS100A9 VLPs were precipitated by adding 10% (w/v) PEG8000 (Thermo Fisher Scientific) at 4 °C for 12 h. The precipitated fraction was pelleted by centrifugation (5000 × *g*, 10 min, 4 °C) and dissolved in phosphate-buffered saline (PBS; 137 mM NaCl, 2.7 mM KCl, 10 mM Na_2HPO_4, 1.8 mM KH_2PO_4, pH 7.4) and then extracted with 0.5 volumes of 1:1 (v/v) butanol/chloroform. The aqueous fraction containing VLPs was separated by centrifugation (5000 × *g*, 10 min, 4 °C) and pure VLPs were recovered by 10−40% sucrose velocity gradient ultracentrifugation (9,6281 × *g*, 2.5 h, 4 °C). The light-scattering VLP band was collected and pelleted by ultracentrifugation (16,0326 × *g*, 2 h, 4 °C) and the pure VLPs were resuspended in PBS and stored at 4 °C until further use.

Characterization of Qβ VLPs.

The VLPs were characterized as previously described[27,28,29]. The VLP concentration was determined using a Pierce BCA assay kit (Thermo Fisher Scientific). To confirm hybrid QβS100A9 assembly and peptide display, 10 μg of QβS100A9 particles was analyzed by SDS-PAGE under reducing conditions on NuPAGE 12% Bis-Tris protein gels (Thermo Fisher Scientific) stained with GelCode Blue Safe protein stain (Thermo Fisher Scientific). The gel images were acquired using the ProteinSimple FluorChem R imaging system, and densitometry was used to determine the number of peptides displayed per hybrid QβS100A9 VLP. The integrity of VLPs was confirmed by TEM using a FEI Tecnai Spirit G2 BioTWIN instrument to examine samples stained with 2% uranyl acetate. FPLC was carried out using an AKTA-FPLC 900 system fitted with Superose 6 Increase 10/300 GL columns (GE Healthcare) using PBS as the mobile phase. Particle size was confirmed by DLS using a Malvern Instruments Zetasizer Nano at 25 °C and plastic disposable cuvettes.

Hot-melt extrusion of VLP-loaded implants.

Implants were prepared from PLGA (Akina; LG ratio = 50:50, molecular weight = 10−15 kDa) using our previously reported desktop melt-processing system[27,28,29,32,33,34]. Briefly, lyophilized QβS100A9 or Qβ VLPs were formulated with the ratio 80% PLGA, 10% VLP and 10% PEG8000 (by weight). The dry components were vortexed and loaded into the hot melt-processing system. The barrel was heated to 70 °C for 90 s, and the piston was set to 10 psi (69 kPa) for extrusion. Implants were stored at room temperature with a desiccant until use.

Immunization of mice.

All animal experiments were approved by the UC San Diego Institutional Animal Care and Use Committee (assurance number D16-00020, protocol number S18021). Eight-week-old female C57BL/6J mice (Jackson Laboratory, #000664) were kept under controlled conditions with food and water provided *ad libitum*. Five animals were assigned to the following four groups: (1) soluble QβS100A9, (2) soluble free peptide (control), (3) QβS100A9 implant, and (4) Qβ implant (control). For soluble formulations, we injected 100 μg of QβS100A9 VLPs or 5 μg of free peptide epitope (synthesized by GenScript Biotech) s.c. in 100 μl of PBS every 2 weeks, making three doses in total (prime + two boosts). The PLGA-based implants were cut into lengths of 0.3–0.5 cm according to their weight to provide 300 μg of QβS100A9 vaccine (to match the 300 μg total dose of the soluble formulation) or unmodified Qβ as control. Implants were placed using an 18G needle (BD Biosciences) s.c. behind the neck. Blood samples were taken by tail bleeding at week 0 (before vaccination) and at multiple time points thereafter. Plasma was separated in lithium/heparin-treated tubes (Thomas Scientific) by centrifugation (2000 × *g*, 10 min, room temperature) and the plasma was stored at −80 °C.

Peptide-specific IgG titers.

Endpoint total IgG titers against the S100A9 peptide epitope were determined by enzyme-linked immunosorbent assay (ELISA)[27,29,34]. We coated 96-well, maleimide-activated plates (Thermo Fisher Scientific) with 2.5 μg cysteine-modified S100A9 peptide (**CGSG**RGHGHSHGKG) in 100 μL coating buffer per well (0.1 M sodium phosphate, 0.15 M sodium chloride, 10 mM EDTA, pH 7.2) overnight at 4 °C. After washing (3 × 5 min) with 200 μL/well PBS + 0.05% (v/v) Tween-20 (PBST), the plates were blocked for 1 h with 1% (w/v) L-cysteine (Sigma-Aldrich). After washing as above, plasma samples from vaccinated animals (two-fold serial dilutions in coating buffer) were added to the plates and incubated for 1 h at room temperature. After washing as above, we added a horseradish peroxidase (HRP)-labeled goat anti-mouse IgG (H+L) secondary antibody (Thermo Fisher Scientific, A16072) diluted 1:5000 in PBST (100 μL/well) and incubated as above. Finally, we added 1-Step Ultra TMB substrate (Thermo Fisher Scientific, 100 μL/well) and stopped the reaction after 5 mins with 100 μL/well 2 M H_2SO_4. The endpoint IgG titers were defined as the reciprocal plasma dilution at which the absorbance at 450 nm exceeded twice the background value (blank wells without a plasma sample).

IgG subclasses and immunoglobulin isotypes.

Pooled samples from weeks 2, 8 and 12 (soluble vaccine) or 5, 10 and 15 (implant vaccine) were diluted 1:1000 in coating buffer and tested as described for the endpoint IgG titers above, but the secondary antibodies were HRP-labeled goat anti-mouse IgG1 (Invitrogen PA174421, diluted 1:5000), IgG2b (Abcam ab97250, diluted 1:5000), IgA (Abcam ab98708, diluted 1:5000), IgE (Invitrogen PA184764, diluted 1:1000), and IgM (Abcam ab97230, diluted 1:5000). The IgG1/IgG2b ratio was used to define the response as Th2-biased (IgG1/IgG2b > 1) or Th1-biased (IgG1/IgG2b < 1).

ELISpot assay.

The ELISpot assay was carried out using a mouse IFN-γ/IL-4 double-color ELISPOT kit (Cellular Technology)[27,29,34]. Briefly, 96-well ELISpot plates were coated with anti-mouse IFN-γ and anti-mouse IL-4 antibodies overnight at 4 °C. Splenocyte suspensions (1×10^6 cells/well) collected from n = 3 mice 4 weeks post-immunization or n = 2 naïve mice were cultured with 100 μL medium alone (negative control), 10 μg free S100A9 peptide, 5 μg recombinant mouse S100A9 protein (R&D Systems), 5 μg unmodified Qβ, or 5 ng PMA/100 ng ionomycin (Sigma-Aldrich, positive control) at 37 °C in a 5% CO_2 atmosphere for 24 h. After washing with PBST, the plates were incubated with fluorescein isothiocyanate (FITC)-labeled anti-mouse IFN-γ (1:1000 dilution) and biotin-labeled anti-mouse IL-4 (1:666 dilution) antibodies for 2 h at room temperature. After washing as above, we added streptavidin alkaline phosphatase (AP, 1:1000 dilution) and anti-FITC-HRP (1:1000 dilution) to each well and incubated for 1 h at room temperature. After a final wash with PBST and a rinse in distilled water, we added the AP substrate and incubated for 15 min at room temperature, then rinsed with distilled water, added the HRP substrate, and incubated for 10 min at room temperature. The plates were rinsed five times with distilled water and air-dried at room temperature overnight. Colored spots were quantified using the Immunospot S6 Entry analyzer. Splenocytes were evaluated per animal and tested at least in duplicate for each stimulant. The results were reported as spot-forming cells (SFC) per 1×10^6 cells.

Dot blot assay.

The C-terminal S100A9 epitope is unique among the S100 family[66] so we used a dot blot assay to confirm the specificity of the antibodies elicited by QβS100A9 particles. We spotted 2 μL (1 μg) of recombinant mouse S100A8, S100A9 or heterodimer S100A8/9 (R&D Systems) onto a nitrocellulose membrane (0.45-μm pore size, GE Healthcare) and blocked with 3% bovine serum albumin (Roche) at room temperature for 1 h, followed by washing with PBST. The membrane was then incubated at room temperature for 1 h with pooled plasma (week 4) from QβS100A9-vaccinated or free-peptide-vaccinated mice (diluted 1:100 in PBS). After another wash with PBST, we incubated the membrane with HRP-labeled goat anti-mouse IgG (diluted 1:5000 in PBST) at room temperature for 1 h. Finally, the membrane was washed as above and incubated with 3,3’-diaminobenzidine (DAB) substrate for 1 min. The development of a brown color indicated specific binding to the S100 proteins.

Liver and kidney biomarkers.

The safety of the QβS100A9 vaccine was determined by detecting plasma biomarkers related to liver and kidney injury. For liver damage, we determined the concentrations of the enzymes AST and ALT using the corresponding activity assay kits (Abcam). For kidney damage, we determined the concentration of KIM-1 using the Mouse KIM-1 ELISA Kit (Abcam). Plasma samples collected and tested at weeks 0 and 12 post-vaccination. The plasma samples were pooled from each group and tested in quadruplicate.

Mouse atherosclerosis model.

To determine the efficacy of our vaccine candidates, they were tested in the ApoE$^{-/-}$ mouse model of atherosclerosis (Jackson Laboratory, #002052). Eight-week-old male ApoE$^{-/-}$ mice were fed on the Envigo TD.88137a western purified atherogenic diet (20–23% milkfat/butterfat, 0.2% total cholesterol, 34% sucrose by weight). The animals were vaccinated as described above with PLGA-based QβS100A9 implants containing 300 μg VLPs, and matching implants containing the same dose of unmodified Qβ VLPs as controls. The mice were fed on a regular diet for 4 weeks post-immunization before switching to the high-fat diet for 20 weeks. Mice were fasted for 4 h and blood was sampled at weeks 0, 2, 4, 8, 12 and 24. Plasma was separated to determine endpoint IgG titers and immunoglobulin isotypes as described above. At the end of the study (week 24), the mice were euthanized by CO_2 asphyxiation followed by exsanguination by cardiac puncture. Aortas were perfused with PBS (pH 7.4) before the thoracic aorta and aortic arch were dissected, fixed with 4% formalin, denuded of connective tissue and processed for oil red O staining. Hearts, livers, kidneys, lungs, spleens, and abdominal fat tissues were weighed and fixed with 4% formalin and embedded in paraffin for further analysis.

Oil red O staining.

Aortas were stained as previously reported[67]. Briefly, cleaned and fixed aortas were placed individually in 1.5-mL tubes and equilibrated in 1 mL 78% methanol by gentle motion on a tilted roller (2 × 5 min). The methanol was then replaced with 1 mL fresh 0.2% oil red O solution and the tissue was incubated at room temperature for 1 h. After staining, the tissue was transferred to a clean tube and washed with 1 mL 78% methanol on the tilted roller (2 × 5 min). Finally, the methanol was replaced with 1 mL PBS and aortas were stored at 4 °C. To visualize and quantify the atherosclerotic lesions, aortas were dissected longitudinally and pinned with the lumen siding facing up on a dissecting dish under a stereomicroscope (VistaVision, 10X). The percentage of atherosclerotic lesions was determined by densitometry using ImageJ v1.44o (http://imagej.nih.gov/ij) and was calculated as follows:

$$\%\ \text{lesion} = (\text{total lesion areas [stained red area]/total aorta area}) * 100$$

Cytokine quantification.

Commercial sandwich ELISA kits were used to measure the concentrations of different cytokines in plasma from QβS100A9-vaccinated and control mice. We used kits for mouse

calprotectin S100A8/9 heterodimer (R&D Systems, DY8596-05), mouse MCP-1 (Abcam, ab208979), mouse IL-1β (Abcam, ab229440) and mouse IL-6 (R&D Systems, M6000B).

Statistical analysis.

Data are presented as means ± standard errors of the mean (SEM), with the number of replicates presented for individual experiments. Differences between groups were analyzed using an unpaired two-tailed t-test. Data were analyzed in GraphPad Prism v6, with $p < 0.05$ defined as the threshold for statistical significance.

Supplementary Material

Refer to Web version on PubMed Central for supplementary material.

Acknowledgments

This work was supported in part by a grant from the National Institute of Health (R01 HL137674 to N.F.S.) and O.A.O.-R. acknowledges the UC MEXUS-CONACYT Postdoctoral Fellowship 2019-2020 number FE-19-58. TOC, Figure 2, 4, and 5 were partially created using Biorender.com

References

1. World Health Organization https://www.who.int/news-room/fact-sheets/detail/cardiovascular-diseases-(cvds) (accessed: 11/01/2021).
2. Gisterå A; Hansson GK The Immunology of Atherosclerosis. Nat Rev Nephrol 2017, 13 (6), 368–380. [PubMed: 28392564]
3. Robinson JG; Heistad DD; Fox KAA Atherosclerosis Stabilization with PCSK-9 Inhibition: An Evolving Concept for Cardiovascular Prevention. Atherosclerosis 2015, 243 (2), 593–597. [PubMed: 26545013]
4. Ridker PM; Everett BM; Thuren T; MacFadyen JG; Chang WH; Ballantyne C; Fonseca F; Nicolau J; Koenig W; Anker SD; Kastelein JJP; Cornel JH; Pais P; Pella D; Genest J; Cifkova R; Lorenzatti A; Forster T; Kobalava Z; Vida-Simiti L; Flather M; Shimokawa H; Ogawa H; Dellborg M; Rossi PRF; Troquay RPT; Libby P; Glynn RJ Antiinflammatory Therapy with Canakinumab for Atherosclerotic Disease. New England Journal of Medicine 2017, 377 (12), 1119–1131. [PubMed: 28845751]
5. Boekholdt SM; Hovingh GK; Mora S; Arsenault BJ; Amarenco P; Pedersen TR; LaRosa JC; Waters DD; DeMicco DA; Simes RJ; Keech AC; Colquhoun D; Hitman GA; Betteridge DJ; Clearfield MB; Downs JR; Colhoun HM; Gotto AM; Ridker PM; Grundy SM; Kastelein JJP Very Low Levels of Atherogenic Lipoproteins and the Risk for Cardiovascular Events: A Meta-Analysis of Statin Trials. Journal of the American College of Cardiology 2014, 64 (5), 485–494. [PubMed: 25082583]
6. Tousoulis D; Oikonomou E; Economou EK; Crea F; Kaski JC Inflammatory Cytokines in Atherosclerosis: Current Therapeutic Approaches. Eur Heart J 2016, 37 (22), 1723–1732. [PubMed: 26843277]
7. Tedgui A; Mallat Z Cytokines in Atherosclerosis: Pathogenic and Regulatory Pathways. Physiol Rev 2006, 86 (2), 515–581. [PubMed: 16601268]
8. Wang S; Song R; Wang Z; Jing Z; Wang S; Ma J S100A8/A9 in Inflammation. Frontiers in Immunology 2018, 9.
9. Hessian PA; Edgeworth J; Hogg N MRP-8 and MRP-14, Two Abundant Ca(2+)-Binding Proteins of Neutrophils and Monocytes. J Leukoc Biol 1993, 53 (2), 197–204. [PubMed: 8445331]
10. Vogl T; Tenbrock K; Ludwig S; Leukert N; Ehrhardt C; van Zoelen MAD; Nacken W; Foell D; van der Poll T; Sorg C; Roth J Mrp8 and Mrp14 Are Endogenous Activators of Toll-like Receptor 4, Promoting Lethal, Endotoxin-Induced Shock. Nat Med 2007, 13 (9), 1042–1049. [PubMed: 17767165]

11. Boyd JH; Kan B; Roberts H; Wang Y; Walley KR S100A8 and S100A9 Mediate Endotoxin-Induced Cardiomyocyte Dysfunction via the Receptor for Advanced Glycation End Products. Circ Res 2008, 102 (10), 1239–1246. [PubMed: 18403730]
12. Hibino T; Sakaguchi M; Miyamoto S; Yamamoto M; Motoyama A; Hosoi J; Shimokata T; Ito T; Tsuboi R; Huh N-H S100A9 Is a Novel Ligand of EMMPRIN That Promotes Melanoma Metastasis. Cancer Res 2013, 73 (1), 172–183. [PubMed: 23135911]
13. Altwegg LA; Neidhart M; Hersberger M; Müller S; Eberli FR; Corti R; Roffi M; Sütsch G; Gay S; von Eckardstein A; Wischnewsky MB; Lüscher TF; Maier W Myeloid-Related Protein 8/14 Complex Is Released by Monocytes and Granulocytes at the Site of Coronary Occlusion: A Novel, Early, and Sensitive Marker of Acute Coronary Syndromes. Eur Heart J 2007, 28 (8), 941–948. [PubMed: 17387139]
14. Healy AM; Pickard MD; Pradhan AD; Wang Y; Chen Z; Croce K; Sakuma M; Shi C; Zago AC; Garasic J; Damokosh AI; Dowie TL; Poisson L; Lillie J; Libby P; Ridker PM; Simon DI Platelet Expression Profiling and Clinical Validation of Myeloid-Related Protein-14 as a Novel Determinant of Cardiovascular Events. Circulation 2006, 113 (19), 2278–2284. [PubMed: 16682612]
15. Katashima T; Naruko T; Terasaki F; Fujita M; Otsuka K; Murakami S; Sato A; Hiroe M; Ikura Y; Ueda M; Ikemoto M; Kitaura Y Enhanced Expression of the S100A8/A9 Complex in Acute Myocardial Infarction Patients. Circ J 2010, 74 (4), 741–748. [PubMed: 20190427]
16. Ionita MG; Vink A; Dijke IE; Laman JD; Peeters W; van der Kraak PH; Moll FL; de Vries J-PPM; Pasterkamp G; de Kleijn DPV High Levels of Myeloid-Related Protein 14 in Human Atherosclerotic Plaques Correlate with the Characteristics of Rupture-Prone Lesions. Arterioscler Thromb Vasc Biol 2009, 29 (8), 1220–1227. [PubMed: 19520974]
17. Kunutsor SK; Flores-Guerrero JL; Kieneker LM; Nilsen T; Hidden C; Sundrehagen E; Seidu S; Dullaart RPF; Bakker SJL Plasma Calprotectin and Risk of Cardiovascular Disease: Findings from the PREVEND Prospective Cohort Study. Atherosclerosis 2018, 275, 205–213. [PubMed: 29957458]
18. Croce K; Gao H; Wang Y; Mooroka T; Sakuma M; Shi C; Sukhova GK; Packard RRS; Hogg N; Libby P; Simon DI Myeloid-Related Protein-8/14 Is Critical for the Biological Response to Vascular Injury. Circulation 2009, 120 (5), 427–436. [PubMed: 19620505]
19. Hobbs JAR; May R; Tanousis K; McNeill E; Mathies M; Gebhardt C; Henderson R; Robinson MJ; Hogg N Myeloid Cell Function in MRP-14 (S100A9) Null Mice. Mol Cell Biol 2003, 23 (7), 2564–2576. [PubMed: 12640137]
20. Ridker PM; Everett BM; Thuren T; MacFadyen JG; Chang WH; Ballantyne C; Fonseca F; Nicolau J; Koenig W; Anker SD; Kastelein JJP; Cornel JH; Pais P; Pella D; Genest J; Cifkova R; Lorenzatti A; Forster T; Kobalava Z; Vida-Simiti L; Flather M; Shimokawa H; Ogawa H; Dellborg M; Rossi PRF; Troquay RPT; Libby P; Glynn RJ Antiinflammatory Therapy with Canakinumab for Atherosclerotic Disease. New England Journal of Medicine 2017, 377 (12), 1119–1131. [PubMed: 28845751]
21. Ljung L; Rantapää-Dahlqvist S; Jacobsson LTH; Askling J Response to Biological Treatment and Subsequent Risk of Coronary Events in Rheumatoid Arthritis. Ann Rheum Dis 2016, 75 (12), 2087–2094. [PubMed: 26984007]
22. Sabatine MS; Giugliano RP; Wiviott SD; Raal FJ; Blom DJ; Robinson J; Ballantyne CM; Somaratne R; Legg J; Wasserman SM; Scott R; Koren MJ; Stein EA; Open-Label Study of Long-Term Evaluation against LDL Cholesterol (OSLER) Investigators. Efficacy and Safety of Evolocumab in Reducing Lipids and Cardiovascular Events. N Engl J Med 2015, 372 (16), 1500–1509. [PubMed: 25773607]
23. Robinson JG; Farnier M; Krempf M; Bergeron J; Luc G; Averna M; Stroes ES; Langslet G; Raal FJ; El Shahawy M; Koren MJ; Lepor NE; Lorenzato C; Pordy R; Chaudhari U; Kastelein JJP; ODYSSEY LONG TERM Investigators. Efficacy and Safety of Alirocumab in Reducing Lipids and Cardiovascular Events. N Engl J Med 2015, 372 (16), 1489–1499. [PubMed: 25773378]
24. Nissen SE; Stroes E; Dent-Acosta RE; Rosenson RS; Lehman SJ; Sattar N; Preiss D; Bruckert E; Češka R; Lepor N; Ballantyne CM; Gouni-Berthold I; Elliott M; Brennan DM; Wasserman SM; Somaratne R; Scott R; Stein EA; for the GAUSS-3 Investigators. Efficacy and Tolerability

of Evolocumab vs Ezetimibe in Patients With Muscle-Related Statin Intolerance: The GAUSS-3 Randomized Clinical Trial. JAMA 2016, 315 (15), 1580–1590. [PubMed: 27039291]

25. ICER, Institute for Clinical and Economic Review. PCSK9 Inhibitors for Treatment of High Cholesterol: Effectiveness, Value, and ValueBased Price Benchmarks Final Report https://icer.org/assessment/high-cholesterol-2015/ (accessed: 11/01/2021)
26. Nilsson J; Hansson GK Vaccination Strategies and Immune Modulation of Atherosclerosis. Circ Res 2020, 126 (9), 1281–1296. [PubMed: 32324498]
27. Ortega-Rivera OA; Pokorski JK; Steinmetz NF A Single-Dose, Implant-Based, Trivalent Virus-like Particle Vaccine against “Cholesterol Checkpoint” Proteins. Advanced Therapeutics 2021, 4 (8), 2100014. [PubMed: 34541299]
28. Shao S; Ortega-Rivera OA; Ray S; Pokorski JK; Steinmetz NF A Scalable Manufacturing Approach to Single Dose Vaccination against HPV. Vaccines 2021, 9 (1), 66. [PubMed: 33478147]
29. Ortega-Rivera OA; Shin MD; Chen A; Beiss V; Moreno-Gonzalez MA; Lopez-Ramirez MA; Reynoso M; Wang H; Hurst BL; Wang J; Pokorski JK; Steinmetz NF Trivalent Subunit Vaccine Candidates for COVID-19 and Their Delivery Devices. J. Am. Chem. Soc 2021, 143 (36), 14748–14765. [PubMed: 34490778]
30. Shin MD; Shukla S; Chung YH; Beiss V; Chan SK; Ortega-Rivera OA; Wirth DM; Chen A; Sack M; Pokorski JK; Steinmetz NF COVID-19 Vaccine Development and a Potential Nanomaterial Path Forward. Nat. Nanotechnol 2020, 15 (8), 646–655. [PubMed: 32669664]
31. Bachmann MF; Jennings GT Therapeutic Vaccines for Chronic Diseases: Successes and Technical Challenges. Philos Trans R Soc Lond B Biol Sci 2011, 366 (1579), 2815–2822. [PubMed: 21893545]
32. Lee PW; Shukla S; Wallat JD; Danda C; Steinmetz NF; Maia J; Pokorski JK Biodegradable Viral Nanoparticle/Polymer Implants Prepared via Melt-Processing. ACS Nano 2017, 11 (9), 8777–8789. [PubMed: 28902491]
33. Wirth DM; Pokorski JK Design and Fabrication of a Low-Cost Pilot-Scale Melt-Processing System. Polymer 2019, 181, 121802.
34. Ortega-Rivera OA; Shukla S; Shin MD; Chen A; Beiss V; Moreno-Gonzalez MA; Zheng Y; Clark AE; Carlin AF; Pokorski JK; Steinmetz NF Cowpea Mosaic Virus Nanoparticle Vaccine Candidates Displaying Peptide Epitopes Can Neutralize the Severe Acute Respiratory Syndrome Coronavirus. ACS Infect. Dis 2021, 7 (11), 3096–3110. [PubMed: 34672530]
35. Jespersen MC; Peters B; Nielsen M; Marcatili P BepiPred-2.0: Improving Sequence-Based B-Cell Epitope Prediction Using Conformational Epitopes. Nucleic Acids Res 2017, 45 (W1), W24–W29. [PubMed: 28472356]
36. Kawano T; Shimamura M; Nakagami H; Iso T; Koriyama H; Takeda S; Baba K; Sasaki T; Sakaguchi M; Morishita R; Mochizuki H Therapeutic Vaccine Against S100A9 (S100 Calcium-Binding Protein A9) Inhibits Thrombosis Without Increasing the Risk of Bleeding in Ischemic Stroke in Mice. Hypertension 2018, 72 (6), 1355–1364. [PubMed: 30571223]
37. Pettersen EF; Goddard TD; Huang CC; Couch GS; Greenblatt DM; Meng EC; Ferrin TE UCSF Chimera--a Visualization System for Exploratory Research and Analysis. J Comput Chem 2004, 25 (13), 1605–1612. [PubMed: 15264254]
38. Corbin BD; Seeley EH; Raab A; Feldmann J; Miller MR; Torres VJ; Anderson KL; Dattilo BM; Dunman PM; Gerads R; Caprioli RM; Nacken W; Chazin WJ; Skaar EP Metal Chelation and Inhibition of Bacterial Growth in Tissue Abscesses. Science 2008, 319 (5865), 962–965. [PubMed: 18276893]
39. Sievers F; Wilm A; Dineen D; Gibson TJ; Karplus K; Li W; Lopez R; McWilliam H; Remmert M; Söding J; Thompson JD; Higgins DG Fast, Scalable Generation of High-quality Protein Multiple Sequence Alignments Using Clustal Omega. Mol Syst Biol 2011, 7 (1), 539. [PubMed: 21988835]
40. Bachmann MF; Jennings GT Vaccine Delivery: A Matter of Size, Geometry, Kinetics and Molecular Patterns. Nat Rev Immunol 2010, 10 (11), 787–796. [PubMed: 20948547]
41. Chung YH; Church D; Koellhoffer EC; Osota E; Shukla S; Rybicki EP; Pokorski JK; Steinmetz NF Integrating Plant Molecular Farming and Materials Research for Next-Generation Vaccines. Nat Rev Mater 2021, 1–17.

42. Finkelman FD; Holmes J; Katona IM; Urban JF; Beckmann MP; Park LS; Schooley KA; Coffman RL; Mosmann TR; Paul WE Lymphokine Control of in Vivo Immunoglobulin Isotype Selection. Annu Rev Immunol 1990, 8, 303–333. [PubMed: 1693082]
43. Rittershaus CW; Miller DP; Thomas LJ; Picard MD; Honan CM; Emmett CD; Pettey CL; Adari H; Hammond RA; Beattie DT; Callow AD; Marsh HC; Ryan US Vaccine-Induced Antibodies Inhibit CETP Activity in Vivo and Reduce Aortic Lesions in a Rabbit Model of Atherosclerosis. Arterioscler Thromb Vasc Biol 2000, 20 (9), 2106–2112. [PubMed: 10978256]
44. Pan Y; Zhou Y; Wu H; Chen X; Hu X; Zhang H; Zhou Z; Qiu Z; Liao Y A Therapeutic Peptide Vaccine Against PCSK9. Sci Rep 2017, 7 (1), 12534. [PubMed: 28970592]
45. Kawakami R; Nozato Y; Nakagami H; Ikeda Y; Shimamura M; Yoshida S; Sun J; Kawano T; Takami Y; Noma T; Rakugi H; Minamino T; Morishita R Development of Vaccine for Dyslipidemia Targeted to a Proprotein Convertase Subtilisin/Kexin Type 9 (PCSK9) Epitope in Mice. PLoS One 2018, 13 (2), e0191895. [PubMed: 29438441]
46. Schiopu A; Cotoi OS S100A8 and S100A9: DAMPs at the Crossroads between Innate Immunity, Traditional Risk Factors, and Cardiovascular Disease. Mediators of Inflammation 2013, 2013, e828354.
47. Shabani F; Farasat A; Mahdavi M; Gheibi N Calprotectin (S100A8/S100A9): A Key Protein between Inflammation and Cancer. Inflamm. Res 2018, 67 (10), 801–812. [PubMed: 30083975]
48. Akache B; Weeratna RD; Deora A; Thorn JM; Champion B; Merson JR; Davis HL; McCluskie MJ Anti-IgE Qb-VLP Conjugate Vaccine Self-Adjuvants through Activation of TLR7. Vaccines (Basel) 2016, 4 (1), 3. [PubMed: 26805897]
49. Sabbisetti VS; Waikar SS; Antoine DJ; Smiles A; Wang C; Ravisankar A; Ito K; Sharma S; Ramadesikan S; Lee M; Briskin R; De Jager PL; Ngo TT; Radlinski M; Dear JW; Park KB; Betensky R; Krolewski AS; Bonventre JV Blood Kidney Injury Molecule-1 Is a Biomarker of Acute and Chronic Kidney Injury and Predicts Progression to ESRD in Type I Diabetes. J Am Soc Nephrol 2014, 25 (10), 2177–2186. [PubMed: 24904085]
50. McGill MR The Past and Present of Serum Aminotransferases and the Future of Liver Injury Biomarkers. EXCLI J 2016, 15, 817–828. [PubMed: 28337112]
51. Kollmus H; Fuchs H; Lengger C; Haselimashhadi H; Bogue MA; Östereicher MA; Horsch M; Adler T; Aguilar-Pimentel JA; Amarie OV; Becker L; Beckers J; Calzada-Wack J; Garrett L; Hans W; Hölter SM; Klein-Rodewald T; Maier H; Mayer-Kuckuk P; Miller G; Moreth K; Neff F; Rathkolb B; Rácz I; Rozman J; Spielmann N; Treise I; Busch D; Graw J; Klopstock T; Wolf E; Wurst W; Yildirim AÖ; Mason J; Torres A; Balling R; Mehaan T; Gailus-Durner V; Schughart K; Hrabě de Angelis M A Comprehensive and Comparative Phenotypic Analysis of the Collaborative Founder Strains Identifies New and Known Phenotypes. Mamm Genome 2020, 31 (1), 30–48. [PubMed: 32060626]
52. Ramírez-Zacarías JL; Castro-Muñozledo F; Kuri-Harcuch W Quantitation of Adipose Conversion and Triglycerides by Staining Intracytoplasmic Lipids with Oil Red O. Histochemistry 1992, 97 (6), 493–497. [PubMed: 1385366]
53. Vogl T; Stratis A; Wixler V; Völler T; Thurainayagam S; Jorch SK; Zenker S; Dreiling A; Chakraborty D; Fröhling M; Paruzel P; Wehmeyer C; Hermann S; Papantonopoulou O; Geyer C; Loser K; Schäfers M; Ludwig S; Stoll M; Leanderson T; Schultze JL; König S; Pap T; Roth J Autoinhibitory Regulation of S100A8/S100A9 Alarmin Activity Locally Restricts Sterile Inflammation. J Clin Invest 2018, 128 (5), 1852–1866. [PubMed: 29611822]
54. Vogl T; Ludwig S; Goebeler M; Strey A; Thorey IS; Reichelt R; Foell D; Gerke V; Manitz MP; Nacken W; Werner S; Sorg C; Roth J MRP8 and MRP14 Control Microtubule Reorganization during Transendothelial Migration of Phagocytes. Blood 2004, 104 (13), 4260–4268. [PubMed: 15331440]
55. Hirata A; Kishida K; Nakatsuji H; Hiuge-Shimizu A; Funahashi T; Shimomura I High Serum S100A8/A9 Levels and High Cardiovascular Complication Rate in Type 2 Diabetics with Ultrasonographic Low Carotid Plaque Density. Diabetes Research and Clinical Practice 2012, 97 (1), 82–90. [PubMed: 22333479]
56. Holzinger D; Nippe N; Vogl T; Marketon K; Mysore V; Weinhage T; Dalbeth N; Pool B; Merriman T; Baeten D; Ives A; Busso N; Foell D; Bas S; Gabay C; Roth J Myeloid-Related Proteins 8

and 14 Contribute to Monosodium Urate Monohydrate Crystal-Induced Inflammation in Gout. Arthritis Rheumatol 2014, 66 (5), 1327–1339. [PubMed: 24470119]

57. Nishikawa Y; Kajiura Y; Lew JH; Kido J; Nagata T; Naruishi K Calprotectin Induces IL-6 and MCP-1 Production via Toll-Like Receptor 4 Signaling in Human Gingival Fibroblasts. Journal of Cellular Physiology 2017, 232 (7), 1862–1871. [PubMed: 27925202]
58. Galea J; Armstrong J; Gadsdon P; Holden H; Francis SE; Holt CM Interleukin-1 Beta in Coronary Arteries of Patients with Ischemic Heart Disease. Arterioscler Thromb Vasc Biol 1996, 16 (8), 1000–1006. [PubMed: 8696938]
59. Bevilacqua MP; Pober JS; Majeau GR; Cotran RS; Gimbrone MA Interleukin 1 (IL-1) Induces Biosynthesis and Cell Surface Expression of Procoagulant Activity in Human Vascular Endothelial Cells. J Exp Med 1984, 160 (2), 618–623. [PubMed: 6332168]
60. Bevilacqua MP; Pober JS; Wheeler ME; Cotran RS; Gimbrone MA Interleukin 1 Acts on Cultured Human Vascular Endothelium to Increase the Adhesion of Polymorphonuclear Leukocytes, Monocytes, and Related Leukocyte Cell Lines. J Clin Invest 1985, 76 (5), 2003–2011. [PubMed: 3877078]
61. Grebe A; Hoss F; Latz E NLRP3 Inflammasome and the IL-1 Pathway in Atherosclerosis. Circulation Research 2018, 122 (12), 1722–1740. [PubMed: 29880500]
62. Kirii H; Niwa T; Yamada Y; Wada H; Saito K; Iwakura Y; Asano M; Moriwaki H; Seishima M Lack of Interleukin-1β Decreases the Severity of Atherosclerosis in ApoE-Deficient Mice. Arteriosclerosis, Thrombosis, and Vascular Biology 2003, 23 (4), 656–660. [PubMed: 12615675]
63. Shimamura M; Kaikita K; Nakagami H; Kawano T; Ju N; Hayashi H; Nakamaru R; Yoshida S; Sasaki T; Mochizuki H; Tsujita K; Morishita R Development of Anti-Thrombotic Vaccine against Human S100A9 in Rhesus Monkey. Sci Rep 2021, 11 (1), 11472. [PubMed: 34075153]
64. Ometto F; Friso L; Astorri D; Botsios C; Raffeiner B; Punzi L; Doria A Calprotectin in Rheumatic Diseases. Exp Biol Med (Maywood) 2017, 242 (8), 859–873. [PubMed: 27895095]
65. Brown SD; Fiedler JD; Finn MG Assembly of Hybrid Bacteriophage Qbeta Virus-like Particles. Biochemistry 2009, 48 (47), 11155–11157. [PubMed: 19848414]
66. Sreejit G; Flynn MC; Patil M; Krishnamurthy P; Murphy AJ; Nagareddy PR Chapter Six - S100 Family Proteins in Inflammation and Beyond. In Advances in Clinical Chemistry; Makowski GS, Ed.; Elsevier, 2020; Vol. 98, pp 173–231. [PubMed: 32564786]
67. Andrés-Manzano MJ; Andrés V; Dorado B Oil Red O and Hematoxylin and Eosin Staining for Quantification of Atherosclerosis Burden in Mouse Aorta and Aortic Root. In Methods in Mouse Atherosclerosis; Andrés V, Dorado B, Eds.; Methods in Molecular Biology; Springer: New York, NY, 2015; pp 85–99.

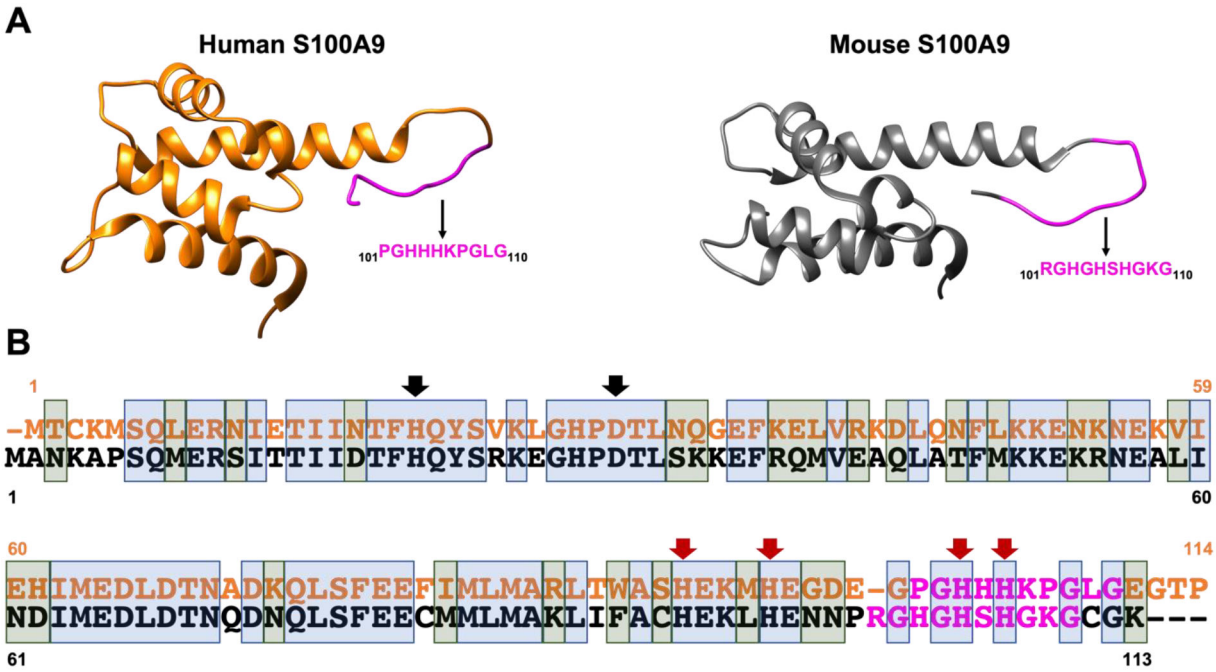

Figure 1.

Similarity between the human and mouse S100A9 proteins. A) Structural models (PDB 6DS2 and 6ZDY). The C-terminal target epitope (residues 101–110) is highlighted in magenta. The structures were rendered using UCSF Chimera[37]. B) Alignment of the human (orange, Uniprot ID P06702) and mouse (black, Uniprot ID P31725) S100A9 amino acid sequences, revealing 58% identity and 74% similarity. Blue boxes indicate fully conserved positions and green boxes indicate chemically similar residues. The two metal-binding sites (S1 and S2) are shown as red and black arrows, respectively[38]. The sequences were aligned using Clustal Omega[39].

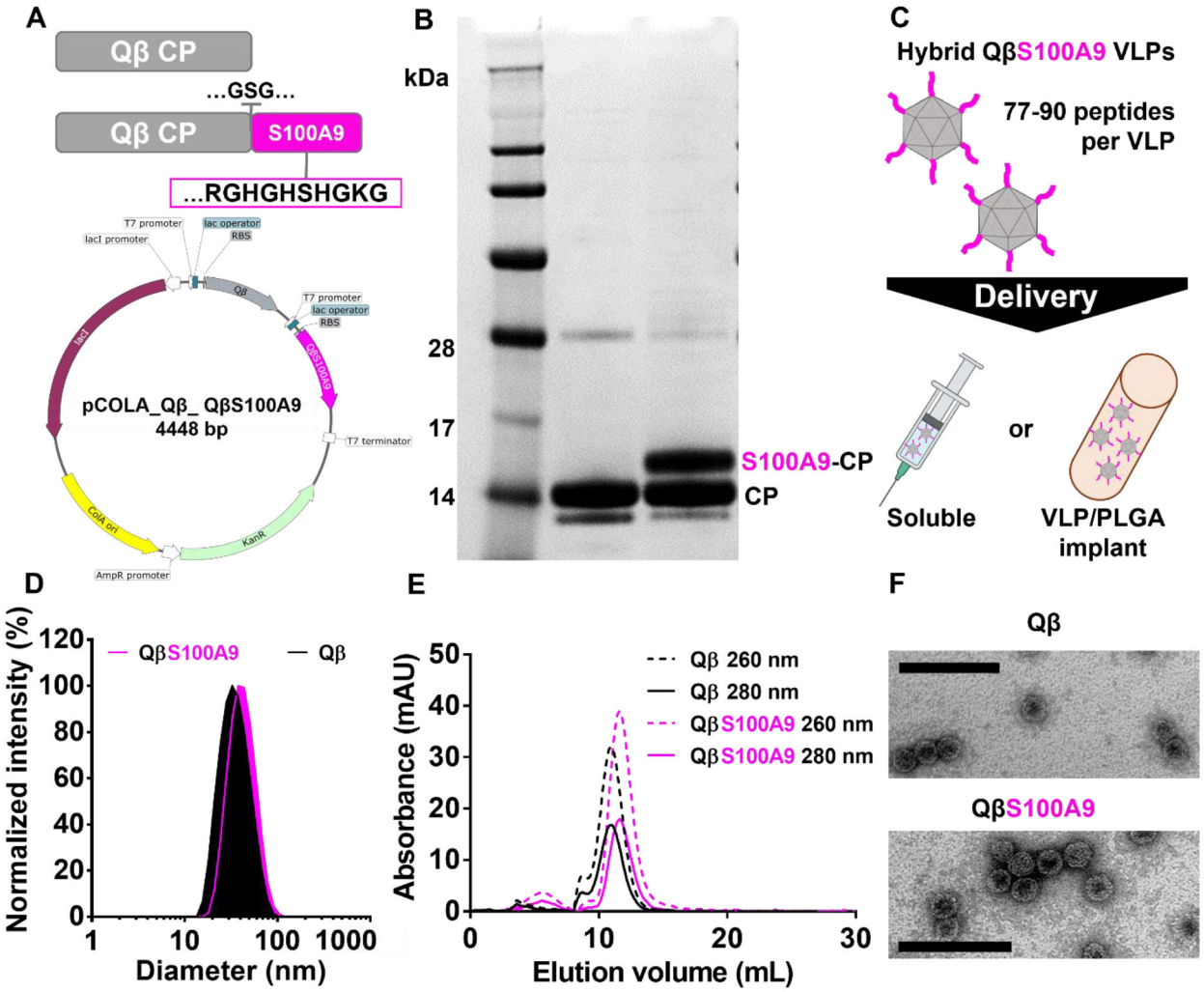

Figure 2.

Production and characterization of QβS100A9 VLPs. A) Schematic (not to scale) of the unmodified Qβ capsid protein (CP) and the QβS100A9 fusion CP with S100A9 epitope $_{101}$RGHGHSHGKG$_{110}$ and an intervening GSG linker, and a map of expression vector pCOLA_Qβ_QβS100A9 with both genes driven by independent T7 promoters and a single T7 terminator (lacI = lactose repressor gene, ColA ori = ColA origin of replication, KanR = kanamycin resistance gene). B) SDS-PAGE analysis of unmodified Qβ (left) and QβS100A9 VLPs (right) under reducing conditions. Unmodified Qβ CP (CP ~14 kDa) and modified QβS100A9 (S100A9-CP ~15.2 kDa) were visualized after staining with GelCode Blue Safe protein stain. C) The number of peptides displayed per hybrid QβS100A9 VLP was determined by densitometry. QβS100A9 VLPs were then used in two delivery formulations (soluble VLPs and slow-release implants). D) DLS of unmodified Qβ and QβS100A9 VLPs shows monodisperse particles. Z-average (dm) = 32.4 ± 0.5 for unmodified Qβ and 39.2 ±0.2 for QβS100A9. PDI = 0.11 for unmodified Qβ and 0.01 for QβS100A9. E) FPLC analysis of unmodified Qβ and QβS100A9 VLPs display similar elution curves. F) TEM images of negatively-stained unmodified Qβ and QβS100A9 VLPs (scale bar = 100 nm). All

samples were tested in triplicate (n = 3) for all characterization methods, and the pictures and data shown are representatives of those triplicates.

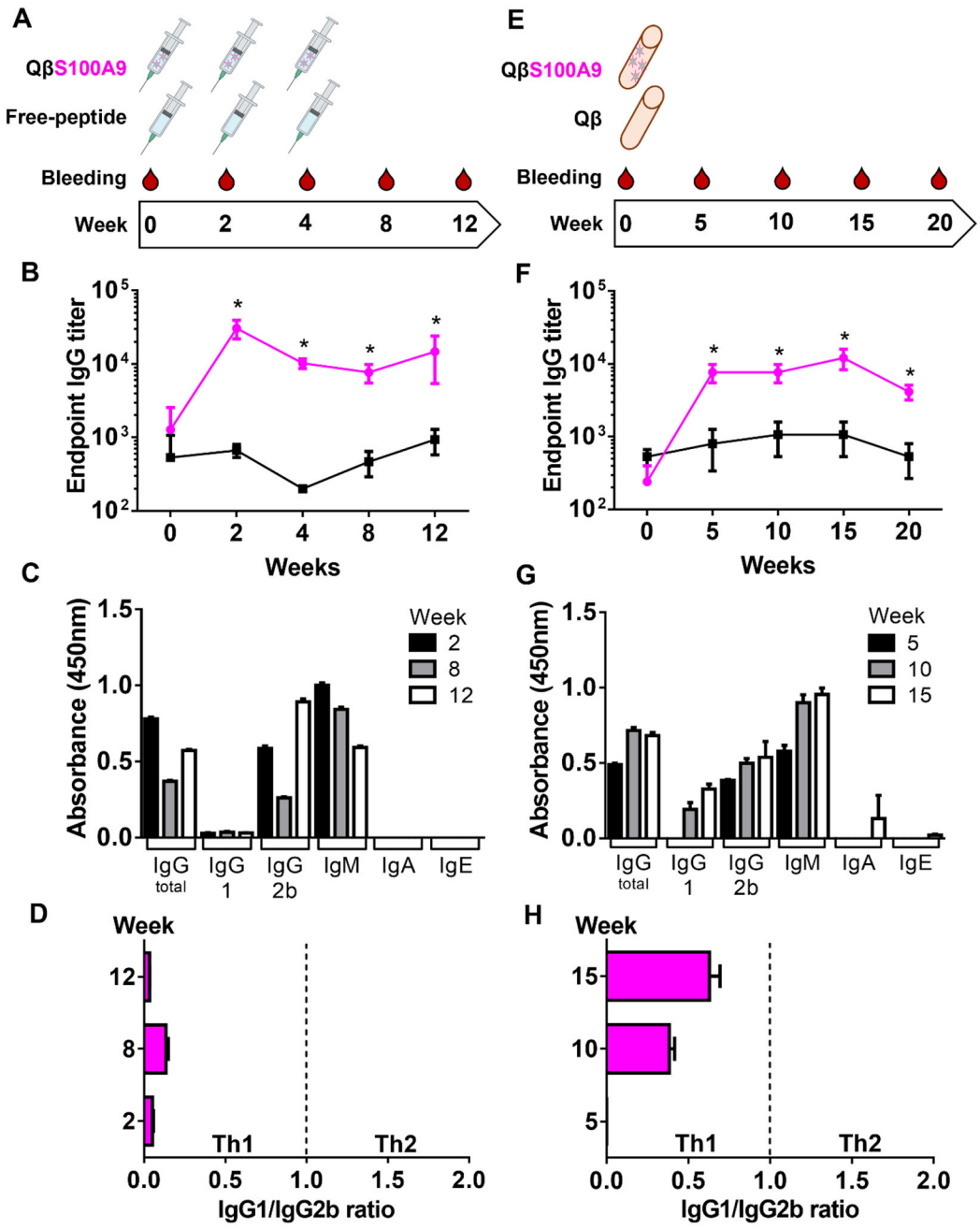

Figure 3.

Immunization of C57Bl6J mice with QβS100A9 vaccines. A) Mice were immunized with 100 μg per injection of the soluble QβS100A9 vaccine or 5 μg of the free peptide (control) in a traditional prime plus two boosts schedule. B) ELISA against S100A9 peptide from the soluble vaccine showing endpoint IgG titers. C) ELISA against S100A9 peptide from the soluble vaccine showing absorbance of IgG subclasses and Ig isotypes over time. D) T-cell helper (Th)-biased profile based on the IgG1/IgG2b ratio of the soluble vaccine. E) Mice were immunized with a PLGA implant containing 300 μg QβS100A9 VLPs (equivalent to the total amount of soluble VLPs) or non-modified Qβ VLPs (control). F) ELISA

against S100A9 peptide from implant vaccine showing endpoint IgG titers. G) ELISA against S100A9 peptide from implant vaccine showing absorbance of IgG subclasses and Ig isotypes over time. H) T-cell helper (Th)-biased profile based on the IgG1/IgG2b ratio of the implant vaccine. Data are means ± SEM (n = 5 biological samples, unpaired two-tailed t-test with 95% confidence value, *$p < 0.05$)

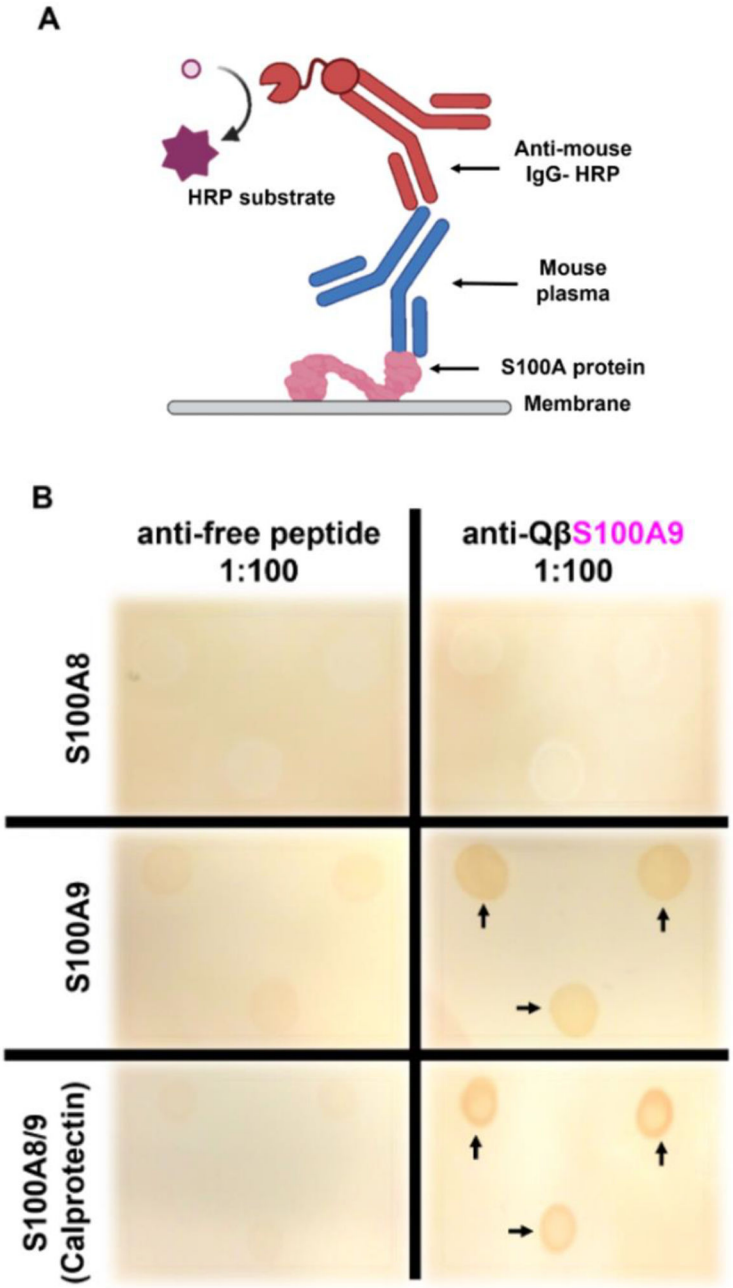

Figure 4.

Specificity of antibodies elicited against the S100A9 epitope displayed on VLPs or as a free peptide. A) Schematic of dot blot immunodetection of S100A8, S100A9, and calprotectin (S100A8/9). B) Pooled plasma (dilution 1:100) from mice vaccinated with QβS100A9 VLPs (right column) or the free peptide (left column) was tested against mouse recombinant S100A8, S100A9 and heterodimer S100A8/9 (calprotectin) by dot blot (1 μg/dot and 3 dots per membrane). Plasma from mice vaccinated with QβS100A9 recognized the S100A9 protein and its heterodimer S100A8/9, but not the S100A8 protein. Black arrows indicate

positive staining. No or barely detectable signal was observed from free-peptide plasma group, as expected.

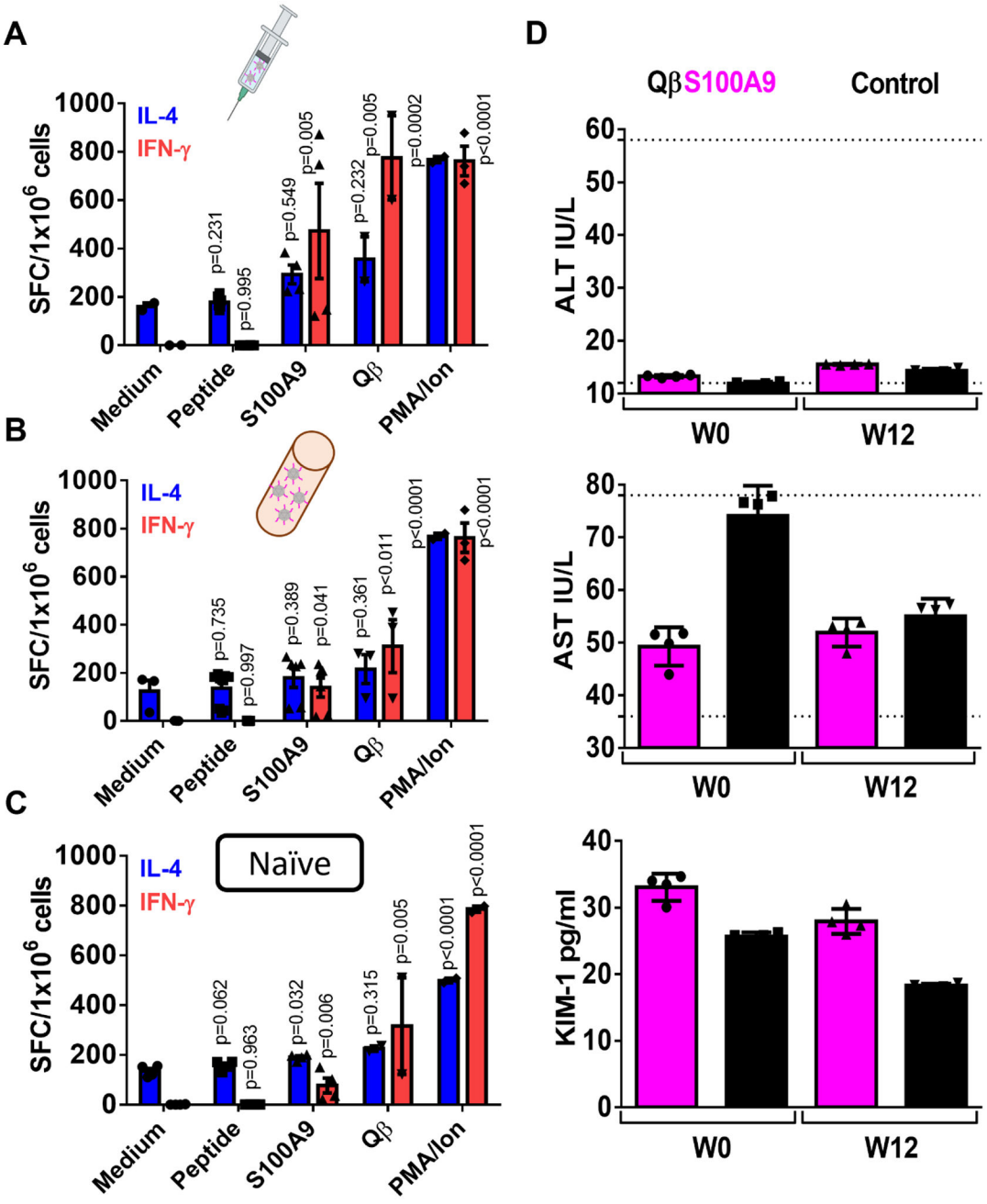

Figure 5.

Plasma biomarkers and ELISpot assays for the analysis of vaccine safety. (A-C) ELISpot assays using splenocytes from mice vaccinated with (A) soluble QβS100A9 VLPs or (B) PLGA-based QβS100A9 implants compared to (C) splenocytes from naïve mice. The splenocytes from each vaccinated (n = 3) or naïve (n = 2) group were cultivated at least in duplicate with medium (negative control), free peptide, whole S100A9 protein, unmodified Qβ VLPs, or PMA/ionomycin (positive control). D) Three plasma biomarkers related to liver injury (AST and ALT) and kidney injury (KIM-1) were evaluated at week 0 (baseline) and week 12 after vaccination (n = 4 from pooled plasma). Dashed lines in the AST and

ALT plots indicate the threshold for normal healthy mice. Data are means ± SEM (unpaired two-tailed t-test with 95% confidence value, *$p < 0.05$).

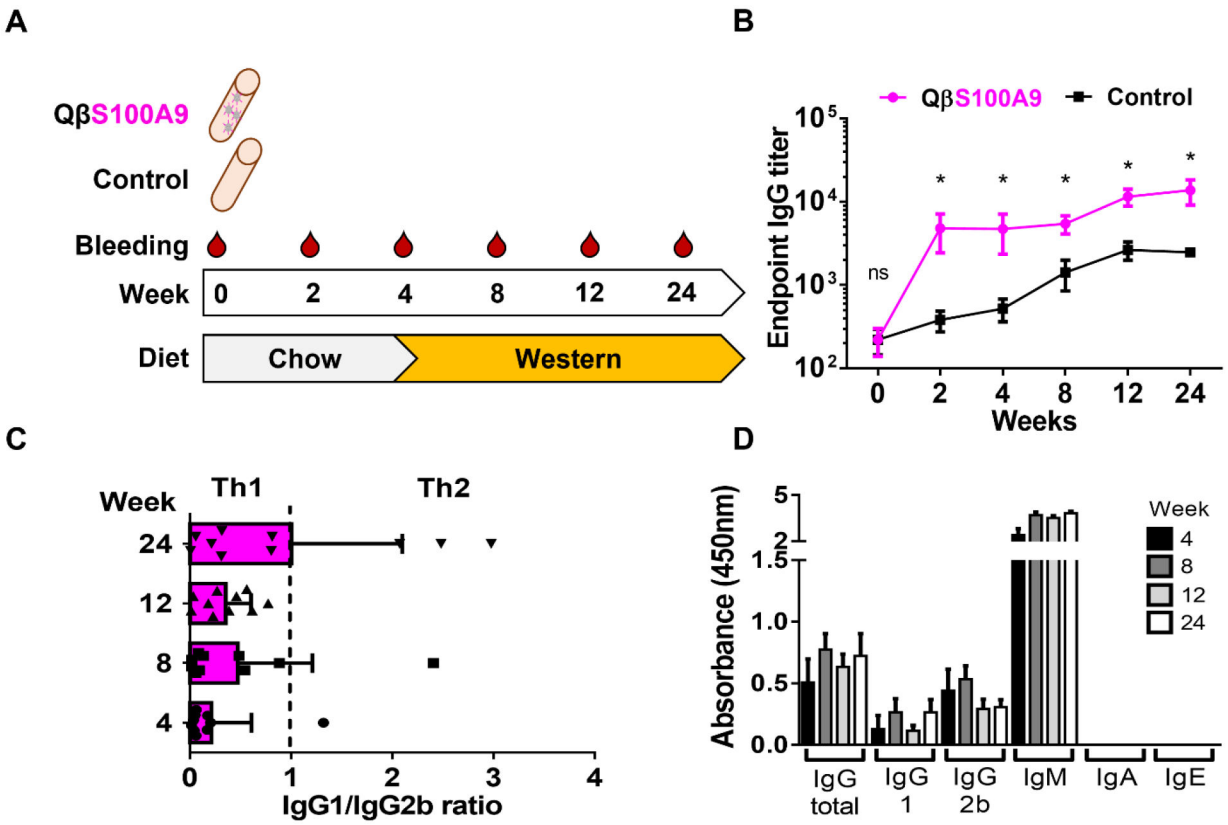

Figure 6.

Immunogenicity of the QβS100A9 vaccine implant in a mouse model of atherosclerosis fed on a high-fat western diet. A) Vaccination and diet schedule for ApoE$^{-/-}$ male mice (n = 10 per group). Two groups were tested, one vaccinated with the QβS100A9 implant (300 μg total dose) and a control group vaccinated with an equivalent dose of unmodified Qβ VLPs. B) Anti-S100A9 peptide antibody titers at different time points after implantation. C) IgG1/IgG2b ratios at four time points to characterize the Th profile (ratio < 1 = Th1-biased, ratio > 1 = Th2-biased). The Th profile shifted from Th1-biased to balanced Th1/Th2 over time. D) Complete immunoglobulin profile over time. Data are means ± SEM (n = 10, unpaired two-tailed t-test with 95% confidence value, *p < 0.0001).

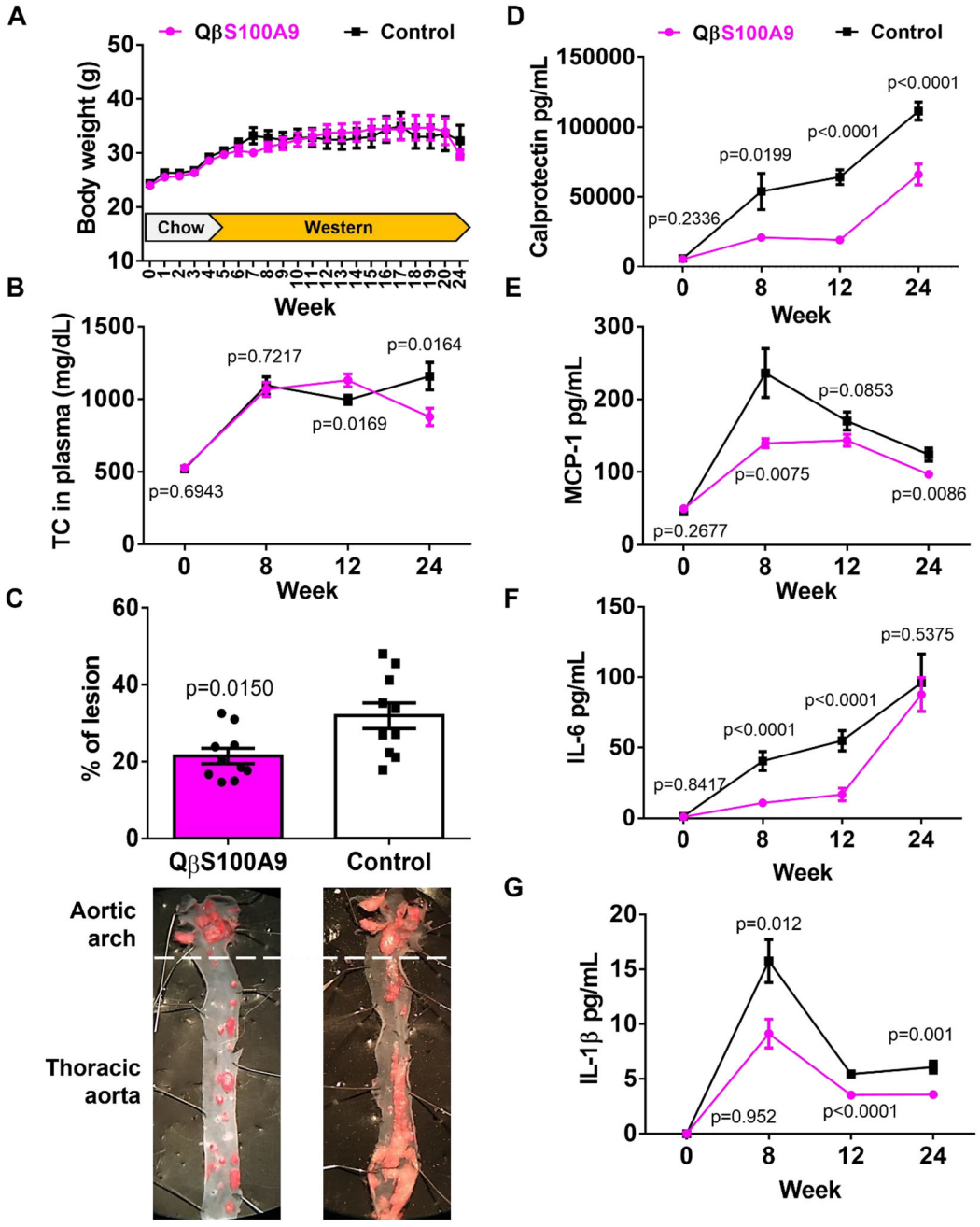

Figure 7.

Effect of QβS100A9 vaccine implants on a mouse model of atherosclerosis fed on a high-fat western diet. A) Body weight (grams) determined weekly. B) Total cholesterol in plasma determined at four time points. C) The presence of atherosclerotic plaques shown as the percentage of lesion determined by oil red O staining. Representative aortic arch and thoracic aorta images from QβS100A9 vaccinated and control groups are shown below, with red areas indicating the atherosclerotic plaques. D-G) Levels of key biomarkers in plasma before (week 0) and after vaccination (weeks 8, 12 and 24): D) calprotectin, E) monocyte chemoattractant protein-1 (MCP-1), F) interleukin-6 (IL-6), and G) interleukin-1β (IL-1β).

Data are means ± SEM (n= 10), unpaired two-tailed t-test, 95% confidence value, $p < 0.05$ was considered the threshold for statistical significance vs control group.